Nitrogen-doped Carbon Dots from Kraft Lignin Waste with Inorganic Acid Catalyst and their Brain Cell Imaging Applications

Yixian Pei[‡a], *An-Yi Chang*[‡a], *Xuan Liu*[a], *Hua Wang*[b], *Hongbo Zhang*[c], *Adarsh Radadia*[a], *Yuxin Wang**[a], *William W. Yu**[b] *and Shengnian Wang**[a]

[a]*Chemical Engineering, Institute for Micromanufacturing, Center for Biomedical Engineering and Rehabilitations, Louisiana Tech University, PO Box 10137, Ruston, Louisiana, 71272 USA.*

[b]*Chemistry and Physics, Louisiana State University, Shreveport, Louisiana, 71115, USA.*

[c]*Department of Microbiology and Immunology, LSU Health Sciences Center, Shreveport, Louisiana, 71104, USA*

‡ These authors contribute equally to this work.

* Corresponding authors.

KEYWORDS: Lignin, Carbon dot, Photoluminescence, Inorganic Acid, Coking

ABSTRACT

Carbon quantum dots (C-QDs) show potential to replace traditional semiconductive quantum dots as the next generation of fluorescent probes. We demonstrate here a new C-QD production process using lignin, a high-volume but low market-value industrial waste and/or environmental hazards, as the starting carbon source. By adding a small amount of inorganic acid, the rich phenolic components in lignin were successfully converted to C-QDs through a coking formation mechanism similar to what happens on solid acid catalysts in traditional fossil fuel cracking process. Their aqueous solution presence of the received lignin C-QDs is beneficial for brain cell imaging applications, attributing to their fast internalization, low toxicity, tunable photoluminescence by appropriate acidity and reaction temperature during hydrothermal synthesis. This method not only provides a low-cost C-QDs production route, but also helps gain extra profit and/or improve environment for many small agricultural business and paper and pulp industry located in rural area.

1. Introduction

Carbon quantum dots (C-QDs) are projected as the new generation of fluorescent probes for their multiple advantages over traditional semiconductive quantum dots counterparts such as excellent biocompatibility, operator-friendly synthesis process, and great environmental sustainability [1]. Many C-QDs synthesis methods, either through physical breakdown of large carbon pieces or hydrothermal synthesis with starting materials varying from coal to small carbonaceous chemicals, have been developed in the past decade [2-11]. C-QDs produced by these processes are often tied with certain luminescence applications varying from sensors [12-14], biological and medical imaging [15-17], LED color display, and lighting devices [18-26]. Despite their success in C-QDs production and application demonstrations, most of early synthesis methods are often involved either multiple steps or expensive and/or toxic carbon sources. Although new synthesis routes using low-cost and/or natural carbon resources such as biomass waste emerge recently [27-30], many of them still face seasonal or geographical supply fluctuation and limited production capacity varying from milligram to gram scale. For some large-scale applications of C-QDs, such as those serve as solar energy harvesting materials in building-integrated photovoltaics for electricity generation [31] or as luminescent tracers of injection fluids to reveal underground conditions of drilling wells [32], truly industrial-scale production capacity of this new type of fluorescence nanomaterial is needed. Their success heavily relies on two factors: how big the sustainable carbon source supply is and how low the market price of C-QDs goes.

To meet such low-cost production requirement on C-QDs, we here target the use of Kraft lignin as the starting materials of carbon source during the synthesis of C-QDs. Lignin, with a

globule production of ~150 billion pounds/year, is however almost exclusively burned for heating [33]. It has also long been a high-volume by-product and environmental hazard of paper and pulp plants. But the chemical structure of lignin is full of various phenols and related compounds, which could potentially be converted to high-value feedstock and/or fuels [34]. Yet current lignin-to-fuel or feedstock production achieves limited success and one major hindrance comes from the quick deactivation of expensive catalyst due to coke formation as well as the followed separation difficulty and cost on a wide variety of aromatic products. Many aromatic intermediates generated during lignin depolymerisation strongly adsorb on the surface of solid catalyst particles to form polyaromatic species (i.e., coke) similar to what happen in traditional fossil fuel cracking processes. As these aromatic carbonaceous polymerization processes are well known trigged by the strong acidic sites on solid catalyst, we hypothesize that C-QDs may be obtained from lignin when it is transformed in appropriate liquid acid environment. In this way, C-QDs can be produced in very low cost and with a sustained supply of carbon sources. Specifically, lignin is first hydrolyzed under strong agitation, followed by hydrothermal synthesis with addition of appropriate amount of inorganic acid, as schematically shown in Figure 1. With this method, in addition to the reception of valuable C-QDs, lignin hazards that long bother the paper and pulp industry can also be eliminated and converted into valuable products to gain additional profits. In this contribution, we demonstrate how to use a small amount of inorganic acid (e.g., nitric acid) liquid other than some very recent work that use more expensive organic acidic or amino additives in the formation of C-QDs. Unlike the direct involvement of those acidic or amino additive, the nitric acid in this work serves mainly as catalyst to trigue hydrocarbon condensation while some nitrogen atoms were doped in the polyaromatic domains for their favourable surface functions for luminescence. With similar

atomic size and five valence electrons for bonding, the nitrogen doping could change the spin density and charge distribution of the carbon matrix, which thereby enhances the radiation transition probability and the photoluminescence yield of C-QDs [35]. Besides evaluate their chemical and luminescent properties, we also explored the cell uptake, toxicity, and imaging performance of these lignin derived C-QDs in N27 rat dopaminergic neural cell line for potential brain imaging applications.

2. Materials and Methods

2.1 Materials and reagents

Kraft lignin and nitric acid (70%) were purchased from Sigma-Aldrich and used as received without further purification. Deionized water (18 MΩ) generated from Millipore system was used in hydrothermal synthesis. All other chemicals were purchased from Sigma-Aldrich and the cell culture reagents were purchased from Life Technologies (Carlsbad, CA) unless specified.

2. 2 Hydrothermal Synthesis of C-QDs

Lignin (0.25-1.0 g) was first dissolved in DI water under strong agitation (600 rpm) for 4 hours. Appropriate amount of nitric acid (or other inorganic acids) was then added in and the mixture was kept hydrothermally in a PPL-lined autoclave with a temperature range of 140-240°C and a processing time of 8-24 hours. The received dark brown solution was diluted and measured for their fluorescence performance without further purification.

2.3 C-QDs Characterization

The optical properties of C-QDs were measured using photoluminescence spectroscopy (ISS, K2 Multifrequency Phase Fluorometer). The quantum yield (QY) was calculated using quinine sulfate in 0.1M H_2SO_4 (Φ = 54.6%) as the reference using the following equation [36]:

$$QYs/QYr = (Ar/As)(Is/Ir)\times 100\%$$

where A is the absorbance, and I is the integral area of fluorescence peak. The subscript r stands for the reference and s for the sample.

The size and structure of C-QDs were characterized by transmission electron microscopy (TEM, JEOL 1400, JEOL) and high-resolution TEM (HRTEM, Hitachi H-9500, Hitachi). The height of C-QDs was measured on an AGILENT 5420 Atomic Force Microscope (AFM). Fourier transform infrared spectra (FTIR) of dried C-QDs were recorded to identify the functional groups on the surface of C-QDs (Thermo Scientific SMART FTIR spectrometer). The X-ray photoelectron spectroscopy (Scienta Omicron XPS) analysis was done to reveal the chemical state of the as-synthesized C-QDs. The structural purity of C-QDs was examined by laser Raman spectroscopy (HORIBA Scientific XploRA™ PLUS) with a wavelength of 532 nm.

2.4 Mammalian Cell Delivery Tests

N27 rat dopaminergic neural cells (Millipore, SCC048) were cultured in RPMI 1640 media supplemented with 10% heat-inactivated fetal bovine serum (FBS), 100 U/mL penicillin, 100 µg/mL streptomycin, and L-glutamine. Cells were maintained in T-75 flasks at 37 °C with 5% CO_2 and digested using 0.25% (w/v) trypsin with EDTA·4Na during subculture.

Cells were first centrifuged and re-suspended in fresh OPTI-MEM I (a serum free medium) at a density of 0.5×10^7 cells/ml. Samples were then mixed with C-QDs solutions of various concentrations (prepared by either concentrating or diluting from the synthesis solution)

and incubated for an hour. The uptake of C-QDs and their potential impact on cell morphology were evaluated quantitatively by a flow cytometry (CytoFLEX, Beckman Coulter). The fluorescence intensity of C-QDs in cells was measured. At least 10,000 events were collected for each sample. CytExpert software was used for all data analysis. The uptake efficiency of C-QDs is defined as the percentage of cells emitting green fluorescence signal among all counted cells in a sample (gated fluorescence signal).

The cell viability was evaluated by an MTS assay (Promega, Madison, WI) after one-day incubation of cells with C-QDs in culture medium. This proliferation-based cell viability evaluation helps reveal the potential disturbance of C-QDs on cell metabolic activity. For each assay, cells of 100 µl from every sample were transferred to a 96-well plate. CellTiter 96 AQueous One solution (Promega, Madison, WI) of 20 µl was added to each well and all samples were incubated at 37°C for another 4 hr. Absorbance was measured at 492 nm on an automated plate reader (Elx 800, Biotek, VT). The cell viability is calculated as the absorbance signal ratio of a treated cell sample to that of the negative control cell sample (without incubation with C-QDs) in MTS assay, after extracting the absorbance background from the media. Data points were represented as the mean ± standard deviation (SD) of triplicates, unless otherwise indicated.

Cellular uptake of C-QDs and their distribution in N27 cells were examined by laser scanning confocal microscopy. Cells were seeded on cover clips in culturing wells one day prior to imaging. C-QDs were then introduced and incubated with cells for an hour, followed by washing twice with 1X PBS. Cell nuclei were then stained with 20 µM of DAPI. Images of blue and UV laser channel channels were taken on a Zeiss 510 META Laser Scanning Confocal microscopy and then merged images were produced using the LSM Imaging software.

3. Results and Discussions

3.1 Synthesis of Lignin C-QDs

The morphology of the C-QDs was characterized by atomic force microscopy (AFM) and transmission electron microscopy (TEM). As shown in Figures 2a & 2b, the lignin CDs have a diameter varying from 3 to 6 nm and an average diameter of 4.6 nm. The AFM image of C-QDs gives a topographic height of C-QDs ~3-6 nm (Figure 2a), indicating their nearly spherical geometry. The high-resolution TEM (HRTEM) image shows that the received C-QDs have clear crystalline lattice fringes (Figure 2c), with one major lattice spacing of 0.21 nm, attributed to the (100) in-plane lattice of graphene [37]. Unlike many other C-QDs synthesized through natural materials, these lignin derived C-QDs have crystalline pattern spread over the whole particles (Figure 2c). Even within some existing C-QDs clusters, such lattice fringes are clearly seen, suggesting that those clusters are assembled C-QDs individuals, not lignin debris after incomplete transformation. The strong signal and well-defined pattern from electron diffraction further confirm their highly crystallized structure (inset of Figure 2c).

XPS survey scan results of lignin and synthesized C-QDs clearly reveal that the major elements of lignin Q-CDs are carbon and oxygen (C 1s: 50.3 at%; O 1s: 36.3 at%), similar to what are in lignin (Figure 3a). However, when compared to lignin, the oxygen percentage in lignin C-QDs is reduced from 46.1at% to 36.3at%, together with a great increase of carbon percentage from ~25.0 at% to 50.3 at%. The Na KLL Auger peak at 497eV disappears after nitric acid catalyzed hydrothermal treatment, suggesting that sodium carbonate compounds in lignin samples were leached out completely. The detailed scan result of O 1s also confirms this conclusion with the disappearance of overlapped Na Auger peak at 536 eV (Figure 3b and supp Figure 1). But some nonmetallic elements such as sulfur in lignin retain in the produced lignin

derivate C-QDs (Figure 3a). The detailed scan of C1s reveals the significant signal reduction of the C 1s peak located between 288-289 eV (Figures 3b and supp Figure 2), which is associated with C=O, O-C=O, and O-C-O groups. Deconvolution of O 1s and C 1s peaks indicates the increase of C-OH groups (533eV for O 1s, 286.9 eV for C 1s) besides the dominated O 1s peak at 531 eV (C=O and O-C=O) and the C 1s peak at 284.8eV (sp2 C=C), as shown in Figures 3b & 3c and supp Figures 1&2. This indicates the loss of many ether bonds that bridge benzene rings between individual units of lignin structure during the six-carbon ring packing process. As nitric acid was used as catalyst, nitrogen element was also successfully introduced in C-QDs with an atomic weight of 3.7 at% (Figure 3a). The high-resolution spectrum of N 1s (Figure 3d) reveals two deconvoluted peaks identified at 401.7 and 402.2 eV (supp Figure 3). This indicates that the nitrogen-containing groups in this Kraft lignin derived C-QDs are presented in the graphitic nitrogen bond (C-NH) and oxidized nitrogen bond (C-N=O). No deep oxidized peaks such as oxidized pyridine nitrogen (near 404 eV) and -NO_2 groups (near 405 eV) were seen. These observations are in consistent with the increase of C-N peak (near 286.0 eV) in the C1s spectrum. The XPS results clearly indicate that C-QDs doped with nitrogen atoms were successfully synthesized from Kraft lignin and their surface are functionalized with C-OH, COOH, C-NH, and C-N=O groups.

FT-IR spectra (Figure 4a) show that the major stretching vibration peaks of lignin are still retained in the lignin C-QDs, suggesting the similar surface functional groups. However, the major stretching peaks for C-H (at 823 cm^{-1}), C=C bending (990 cm^{-1}), C-O stretching (1107 cm^{-1} and 1348 cm^{-1}) and C=O (1558 cm^{-1}) as well as a broad peak of O-H group (2900-3020 cm^{-1}) become more obvious in lignin C-QDs than that in lignin itself. This suggests the formation of more multiple-carbon rings after the disappearance of many C-O-C linkages commonly seen in

lignin. Peaks of the stretching vibration of C=N bonds (1753 cm^{-1}) and N-H bonds (3380 cm^{-1}), though weak, also appear on the lignin C-QDs' spectra. This suggests successful integration of nitrogen element in C-QDs, either in surface functional groups or in the multiple-carbon rings. In Raman spectra (Figure 4b), a sharp band (at 1452 cm^{-1}) contributed to CH_3 bending in OCH_3 is clearly shown in the lignin sample, which is replaced with a broader band or multiple overlapped bands indicates a mixture of various bending modes of CH_x and aromatic ring vibrations there in lignin C-QDs sample. Nevertheless, the typical D band at 1355 cm^{-1} and G band at 1598 cm^{-1} in carbon crystals show up in the C-QDs derived from lignin, corresponding to the disordered structure and the graphitic carbon domain respectively. Their well-defined D band and G band peaks with an intensity ratio (I_D/I_G) close to 1.5 is quite impressive C-QDs Raman data.

3.2 Photoluminescence Analysis of Lignin C-QDs

The photoluminescence was measured on as-prepared lignin C-QDs and their diluted samples. The as-prepared sample shows low luminescence signal with a broad emission peak centered near 460 nm due to its too high the concentration of C-QDs (Figure 5a). Dilution of the as-prepared lignin C-QDs sample continuously enhances the emitted fluorescence signal intensity until reaching 25% of its original concentration. The corresponding fluorescence quantum yield is calculated to be ~10%, which is comparable to other lignin C-QDs derived from alkali lignin that is relatively easier for depolymerization [30]. Given no further purification step was taken for those samples, this is impressive progress towards industrial-scale production of C-QDs which could satisfy applications such as building energy harvesting or drilling fluid tracing that demand large quantity C-QD supply. The increased emission signal during the sequential dilution is companied with a slight blue shift of the peak center. Under the optimal concentration (i.e., 25% of the original lignin C-QDs sample), the emission peak shows clear

red-shift of the peak center and decay of its fluorescence intensity when the excitation wavelength varies from 360 nm to 460 nm (Figure 5b). Since acid was involved during lignin Q-CDs synthesis, which was not removed from the original sample, dilution of the received lignin C-QDs solutions causes also some pH variations. To evaluate how solution pH value affects the photoluminescence signal, diluted lignin C-QDs samples were further measured at various pH values. As shown in Figures 5c & 5d, with an increase of the pH value of the C-QD solution, the photoluminescence intensity shows quick enhancement until a maximum effect of two folds at pH=9, followed by slight decline afterwards. But the centers of all these emission peaks seem pH independent. This suggests that the aforementioned slight blue shift of those peak positions is not the result of the sequential dilution of the original C-QD samples.

3.3 Hydrothermal Conditions on Lignin C-QDs

One unique feature of this work lies on the use of nitric acid to supply nitrogen atoms to C-QDs, which simultaneously helps break down the ether groups in Kraft Lignin (more difficult when compared to alkali lignin that was used in some literatures [30]) by oxidizing them. The followed polymerization of carbonaceous fragments into a stacked carbon-ring structure under acid environment is close to the coking formation mechanism that takes place in many catalytic reactions. This is conceptual different from other C-QD production work that use organic acid and alkali lignin in which the citric acid molecules offer the carboxyl groups and form multiple-atom ring structure through C-N bonds with the second type reactant molecules with amine groups which also provide nitrogen doping [30]. In coking formation, aromatic carbonaceous polymerization processes are strongly correlated to the acidity of solid catalyst used in those reactions and the reaction temperature. Therefore, it is essential to reveal how the transformation of lignin to C-QDs is affected by the liquid acid environment at different reaction temperature.

As shown in Figure 6a, different from the weak photoluminescence signal from products of hydrothermal synthesis without acid, adding a small amount of nitric acid significantly improves the fluorescence signal intensity of the produced lignin C-QDs. Such enhancement continues with the increase of the acidity of the lignin solution during hydrothermal synthesis, which reaches the maximum at the presence of 4% nitric acid (or 2 mL nitric acid in 50 mL lignin solution). Ever stronger acidity is found unfavorable, leading to the opposite, i.e., decline of the photoluminescence signal. These observations are in consistent with the classic coking formation theories: a strong acidic solution or surface provides needed protons for hydrogen transfer and dehydrogenation of hydrocarbon reactants to promote the condensation and rearrangment of aromatic molecules (in our case, the fragments and basic units of lignin) during hyrothermal reactions; however, too strong the acidic environment could significantly accelerates those reactions, resulting in quick formation of polyaromatic clusters and further agglomerations (in this case, the occurrence of lignin C-QD aggregates). Aggregation leads to the size growth of lignin C-QDs and when it goes beyond the critical quantum photoluminescent dimensions (i.e., several nanometers), photons are trapped in those carbon nanoparticles and quickly fade away so that the lignin C-QDs solution has its photoluminescence intensity decayed.

Besides acidity, the hydrothermal synthesis temperature also plays important roles on the quality of the produced lignin C-QDs. However, unlike the acidity effect, lignin C-QDs produced in a broad temperature range show similar strong photoluminescence signal under the same optimal acidity (i.e., 4% nitric acid in hydrothermal synthesis solution), as shown in Figure 6b. Only when the reaction temperature close to the maximum allowance of autoclaves (i.e., 240^{o}C), the decline of photoluminescence signal was seen. The received solution at that hydrothermal temperature carries more large size carbon particles and their appearance probably offsets the

overall quantum yield like what happens in those solutions that are too acidic. Considering the balance of energy consumption cost and quantum efficiency, low temperature synthesis of lignin C-QDs is more favorable and recommended nonetheless.

3.4 Cell Uptake Tests of C-QDs

C-QDs synthesized from organics or involving organic solvents, lignin Q-CDs produced by our inorganic acid catalyzed reactions can be directly used for cell testing. With ability to cross the blood–brain barrier due to their small size, we explored the uptake, toxicity, and luminenscence performance of these lignin C-QDs in N27 cells (a rat neural cell line used as a dopaminergic neuron model) for potential brain imaging applications. Their cell internalization is found very fast and efficient. With one-hour incubation time, more than 15% of live cells already carry enough lignin C-QDs whose photoluminescence signal measurable using flow cytometry when incubated with the most diluted lignin C-QDs samples (i.e., 1.56% of the as-prepared solution), as shown in Figures 7a. The cell uptake rises rapidly when inceasing the concentration of the as-prepared lignin C-QDs. At a concentration of 6.25% of the as-prepared solution, over 50% lignin Q-CDs positive cells present in N27 cells (a adherent cell representitive). The best uptake occurs with a concentration of 12.5% of the as-prepared solution with over 80% positive cells for N27 cells. Further increase of the lignin C-QD concentration starts showing some negative impact on the cell viability and the drop of C-QD positive cell percentage in live cell subgroups.

To further verify cell toxicity, lignin C-QDs samples with a sequential dilution were prepared, followed by 24-hour incubation with cells. As shown in Figures 7b, N27 cells can tolerate (with a cell viability higher than 60%) to a concentrated lignin Q-CDs solution up to 12.5% of the original solution (i.e., only eight-fold dilution of the as-prepared lignin Q-CD

solution). Further concentrated lignin C-QD solutions (i.e., the as-prepared and less-diluted samples) show obvious cell toxicity.

We also tracked the subcellular distribution of C-QDs after N27 cell internalization using confocal microscope. As shown in Figures 7c, within one hour incubation, many C-QDs have already accumulated in cytoplasm of N27 cells and some were even seen in cell nucelus. This suggests the good permeability of the cell membrane and other membrane of organeles inside cell to those lignin C-QDs. The small size and likely some functional groups on those lignin C-QDs allow their easy transport across these membrane barriers. It is worth to mention that our cell imaging experiments were done with C-QDs in cells on coverslip under culturing status (not fixed cells) in which many ions of different types were still presented. As metal ions are known to quench the photoluminescence from C-QDs, this may cause the quality differences of cellular uptake images shown in this work from what in other similar studies [38, 39].

To further evaluate the interference of metal ions, the fluorescence signal of lignin-derived C-QDs was tested at the presence of Fe^{3+} ions. As shown in supp Figure 4, Fe^{3+} ions have significant quenching effect on the fluorescence intensity of C-QDs. With the gradual increase of the concentration of Fe^{3+} ions from 0 to 500 μM, the fluorescence intensity in the test samples decreases 81%, among which 40% of the fluorescence reduction occurred between samples with 100 μM Fe^{3+} ions and C-QDs alone. This also suggests the potential application of these lignin-derived C-QDs as fluorescence tracers in ion detections like what have been demonstrated in literature [13, 40].

4. Conclusions

In summary, a low-cost C-QD production method is demonstrated using Kraft lignin, a large-volume, low market value waste or environmental hazards as the starting carbon sources. Contributed by its rich phenolic components, lignin was successfully converted to high-value C-QDs with strong photoluminescence signal at the presence of a small amount of inorganic acid, similar to the polyaromatic formation and coking deactivation process that happen in traditional fossil fuel cracking processes. Appropriate acidity and reaction temperature are critical in regulating the size of those received lignin C-QDs and their quantum yield. With their aqueous solution presence, the received lignin C-QDs show low cell toxicity in a broad concentration range. This method provides a new low-cost, sustainable production route of C-QDs using carbon sources from waste and/or environmental hazard of agriculture business and paper and pulp industry. Its success may boost the profit of these business units and improve the environment and economy of many small towns in rural area that has huge lignin resource and needs self-sustainability.

AUTHOR INFORMATION

Corresponding Author

Shengnian Wang: Tel: 1-318-257-5125; Email: swang@latech.edu

William Yu, Tel: 1-318-797-5087; Email: wyu6000@gmail.com

Yuxin Wang, Tel: 1-318-278-0108; Email: w-yuxin@hotmail.com

Author Contributions

The manuscript was written through contributions of all authors. All authors have given approval to the final version of the manuscript. ‡These authors contributed equally.

ACKNOWLEDGMENT

We thank financial support by National Science Foundation Grant [1662735], ACS Petroleum Research Fund [58598-ND10], Louisiana Board of Regent [LEQSF(2019-20)-RD-D-07], and Louisiana Harrelson Family Professorship.

REFERENCES

(1) Baker, S. N.; Baker, G. A. Luminescent carbon nanodots: emergent nanolights. *Angew. Chem. Int Ed* **2010**, *49* (38), 6726–6744.

(2) Li, H.; Kang, Z.; Liu, Y.; Lee, S.-T. Carbon nanodots: synthesis, properties and applications. *Mater. Chem.* **2012**, *22* (46), 24230.

(3) Miao, P.; Han, K.; Tang, Y.; Wang, B.; Lin, T.; Cheng, W. Recent advances in carbon nanodots: synthesis, properties and biomedical applications. *Nanoscale* **2015**, *7* (5), 1586–1595.

(4) Zheng, X. T.; Ananthanarayanan, A.; Luo, K. Q.; Chen, P. Glowing graphene quantum dots and carbon dots: properties, syntheses, and biological applications. *Small* **2014**, *11* (14), 1620–1636.

(5) Liu, H.; Ye, T.; Mao, C. Fluorescent carbon nanoparticles derived from candle soot. *Angew. Chem. Int Ed* **2007**, *46* (34), 6473–6475.

(6) Tian, L.; Ghosh, D.; Chen, W.; Pradhan, S.; Chang, X.; Chen, S. Nanosized carbon particles from natural gas soot. *Chem. Mater.* **2009**, *21* (13), 2803–2809.

(7) Zhu, H.; Wang, X.; Li, Y.; Wang, Z.; Yang, F.; Yang, X. Microwave synthesis of fluorescent carbon nanoparticles with electrochemiluminescence properties. *Chem. Comm.* **2009**, 34, 5118-5120.

(8) Hu, S.-L.; Niu, K.-Y.; Sun, J.; Yang, J.; Zhao, N.-Q.; Du, X.-W. One-step synthesis of fluorescent carbon nanoparticles by laser irradiation. *J. Mater. Chem.* **2009**, *19* (4), 484–488.

(9) Lai, C.-W.; Hsiao, Y.-H.; Peng, Y.-K.; Chou, P.-T. Facile synthesis of highly emissive carbon dots from pyrolysis of glycerol; gram scale production of carbon dots/mSiO2 for cell imaging and drug release. *J. Mater. Chem.* **2012**, *22* (29), 14403-14409.

(10) Ye, R.; Xiang, C.; Lin, J.; Peng, Z.; Huang, K.; Yan, Z.; Cook, N. P.; Samuel, E. L.; Hwang, C.-C.; Ruan, G.; et al. Coal as an abundant source of graphene quantum dots. *Nat. Commun.* **2013**, *4* (1), 2934.

(11) Das, R.; Bandyopadhyay, R.; Pramanik, P. Carbon quantum dots from natural resource: A review. *Materials Today Chemistry* **2018**, *8*, 96–109.

(12) Nie, H.; Li, M.; Li, Q.; Liang, S.; Tan, Y.; Sheng, L.; Shi, W.; Zhang, S. X.-A. Carbon dots with continuously tunable full-color emission and their application in ratiometric pH sensing. *Chem. Mater.* **2014**, *26* (10), 3104–3112.

(13) Sun, C.; Zhang, Y.; Wang, P.; Yang, Y.; Wang, Y.; Xu, J.; Wang, Y.; Yu, W. W. Synthesis of nitrogen and sulfur Co-doped carbon dots from garlic for selective detection of Fe3+. *Nanoscale Res Lett* **2016**, *11* (1), 110.

(14) Shen, P.; Xia, Y. Synthesis-Modification Integration: One-Step fabrication of boronic acid functionalized carbon dots for fluorescent blood sugar sensing. *Anal. Chem.* **2014**, *86* (11), 5323–5329.

(15) Sukhanova, A.; Nabiev, I. Fluorescent nanocrystal quantum dots as medical diagnostic tools. *Expert Opinion on Medical Diagnostics* **2008**, *2* (4), 429–447.

(16) Bui, T. T.; Park, S.-Y. A carbon dot–hemoglobin complex-based biosensor for cholesterol detection. *Green Chemistry* **2016**, *18* (15), 4245–4253.

(17) Yang, S.-T.; Cao, L.; Luo, P. G.; Lu, F.; Wang, X.; Wang, H.; Meziani, M. J.; Liu, Y.; Qi, G.; Sun, Y.-P. Carbon dots for optical imaging in vivo. *J. Am. Chem. Soc.* **2009**, *131* (32), 11308–11309.

(18) Wang, H.; Sun, C.; Chen, X.; Zhang, Y.; Colvin, V. L.; Rice, Q.; Seo, J.; Feng, S.; Wang, S.; Yu, W. W. Excitation wavelength independent visible color emission of carbon dots. *Nanoscale* **2017**, *9* (5), 1909–1915.

(19) Chen, Q.-L.; Wang, C.-F.; Chen, S. One-step synthesis of yellow-emitting carbogenic dots toward white light-emitting diodes. *Mater. Sci.* **2012**, *48* (6), 2352–2357.

(20) Chen, X.; Wang, H.; Zhang, Y.; William, Y. W. Recent advances of carbon dot-based light-emitting diodes. *Nanomedicine & Nanotechnology Open Access* **2017**, 2(2): 000120.

(21) Sun, Y.-P.; Zhou, B.; Lin, Y.; Wang, W.; Fernando, K. A. S.; Pathak, P.; Meziani, M. J.; Harruff, B. A.; Wang, X.; Wang, H.; et al. Quantum-sized carbon dots for bright and colorful photoluminescence. *J. Am. Chem. Soc.* **2006**, *128* (24), 7756–7757.

(22) Yuan, T.; Meng, T.; He, P.; Shi, Y.; Li, Y.; Li, X.; Fan, L.; Yang, S. Carbon quantum dots: an emerging material for optoelectronic applications. *Mater. Chem. C* **2019**, *7* (23), 6820–6835.

(23) Suzuki, K.; Malfatti, L.; Takahashi, M.; Carboni, D.; Messina, F.; Tokudome, Y.; Takemoto, M.; Innocenzi, P. Design of carbon dots photoluminescence through organo-functional silane grafting for solid-state emitting devices. *Scientific Reports* **2017**, *7* (1), 5469.

(24) Chen, X.; Bai, X.; Sun, C.; Su, L.; Wang, Y.; Zhang, Y.; Yu, W. W. High efficient light-emitting diodes based on liquid-type carbon dots. *RSC Advances* **2016**, *6* (99), 96798–96802.

(25) Shuang, E.; Mao, Q.-X.; Wang, J.-H.; Chen, X.-W. Carbon dots with tunable dual emissions: from the mechanism to the specific imaging of endoplasmic reticulum polarity. *Nanoscale* **2020**, *12* (12), 6852–6860.

(26) Prasannan, A.; Imae, T. One-Pot synthesis of fluorescent carbon dots from orange waste peels. *Ind. Eng. Chem. Res.* **2013**, *52* (44), 15673–15678.

(27) Zhao, S.; Lan, M.; Zhu, X.; Xue, H.; Ng, T.-W.; Meng, X.; Lee, C.-S.; Wang, P.; Zhang, W. Green synthesis of bifunctional fluorescent carbon dots from garlic for cellular imaging and free radical scavenging. *ACS Appl. Mater. Interfaces* **2015**, *7* (31), 17054–17060.

(28) Xue, M.; Zhan, Z.; Zou, M.; Zhang, L.; Zhao, S. Green synthesis of stable and biocompatible fluorescent carbon dots from peanut shells for multicolor living cell imaging. *New J. Chem.* **2016**, *40* (2), 1698–1703.

(29) Dager, A.; Uchida, T.; Maekawa, T.; Tachibana, M. Synthesis and characterization of mono-disperse carbon quantum dots from fennel seeds: photoluminescence analysis using machine learning. *Scientific Reports* **2019**, *9* (1), 14004.

(30) Wang, R.; Xia, G.; Zhong, W.; Chen, L.; Chen, L.; Wang, Y.; Min, Y.; Li, K. Direct transformation of lignin into fluorescence-switchable graphene quantum dots and their application in ultrasensitive profiling of a physiological oxidant. *Green Chemistry* **2019**, *21* (12), 3343–3352.

(31) Wu, K.; Li, H.; Klimov, V. I. Tandem luminescent solar concentrators based on engineered quantum dots. *Nat. Photonics* **2018**, *12* (2), 105–110.

(32) Jacoby, M. Seeking to boost oil production, petroleum researchers turn to nanotech. *Chem. & Eng. News*, **2018**, *96*(10), 27-30.

(33) Suhas; Carrott, P.; Carrott, M. R. Lignin – from natural adsorbent to activated carbon: A review. *Bioresource Technology* **2007**, *98* (12), 2301–2312.

(34) Wang, Y.; Song, J.; Baxter, N.; Kuo, G.-T.; Wang, S. Synthesis of hierarchical ZSM-5 zeolites by solid-state crystallization and their catalytic properties, *J. Catal.* **2017**, *349* (5), 53-65.

(35) Wang, H.; Haydel, P.; Wang, L.; Liang, Y.; Yu, W. W. Wide emission shifts and high quantum yields of solvatochromic carbon dots with rich pyrrolic nitrogen, *Nano research* **2020**, *13* (9), 2492–2499.

(36) Jiang, K.; Sun, S.; Zhang, L.; Wang, Y.; Cai, C.; Lin H. Bright-yellow-emissive N-doped carbon dots: preparation, cellular imaging, and bifunctional sensing, *ACS Appl. Mater. Interfaces* **2015**, *7* (41), 23231-23238.

(37) Tang, L.; Ji, R.; Li, X.; Bai, G.; Liu, C. P.; Hao, J.; Lin, J.; Jiang, H.; Teng, K. S.; Yang, Z. Deep ultraviolet to near-infrared emission and photoresponse in layered N-doped graphene quantum dots. *ACS Nano* **2014**, *8*(6), 6312-6320.

(38) Hua, X.-W.; Bao, Y.-W.; Zeng, J.; Wu, F. G. Nucleolus-targeted red emissive carbon dots with polarity-sensitive and excitation-independent fluorescence emission: high-resolution cell imaging and in vivo tracking, *ACS Appl. Mater. Interfaces* **2019**, *11*(36), 32647-32658.

(39) Hua, X.-W.; Bao, Y.-W.; Wu, F. G. Fluorescent carbon quantum dots with intrinsic nucleolus-targeting capability for nucleolus imaging and enhanced cytosolic and nuclear drug delivery, *ACS Appl. Mater. Interfaces* **2018**, *10*(13), 10664

(40) Gao, G.; Jiang, Y.-W.; Jia, H.-R.; Yang, J.; Wu, G.-F. On-off-on fluorescent nanosensor for Fe^{3+} detection and cancer/normal cell differentiation via silicon-doped carbon quantum dots, *Carbon* **2018**, *134* (8), 232-243.

FIGURES CAPTIONS

Figure 1. Schematic of carbon dot synthesis route from lignin under acidic environment.

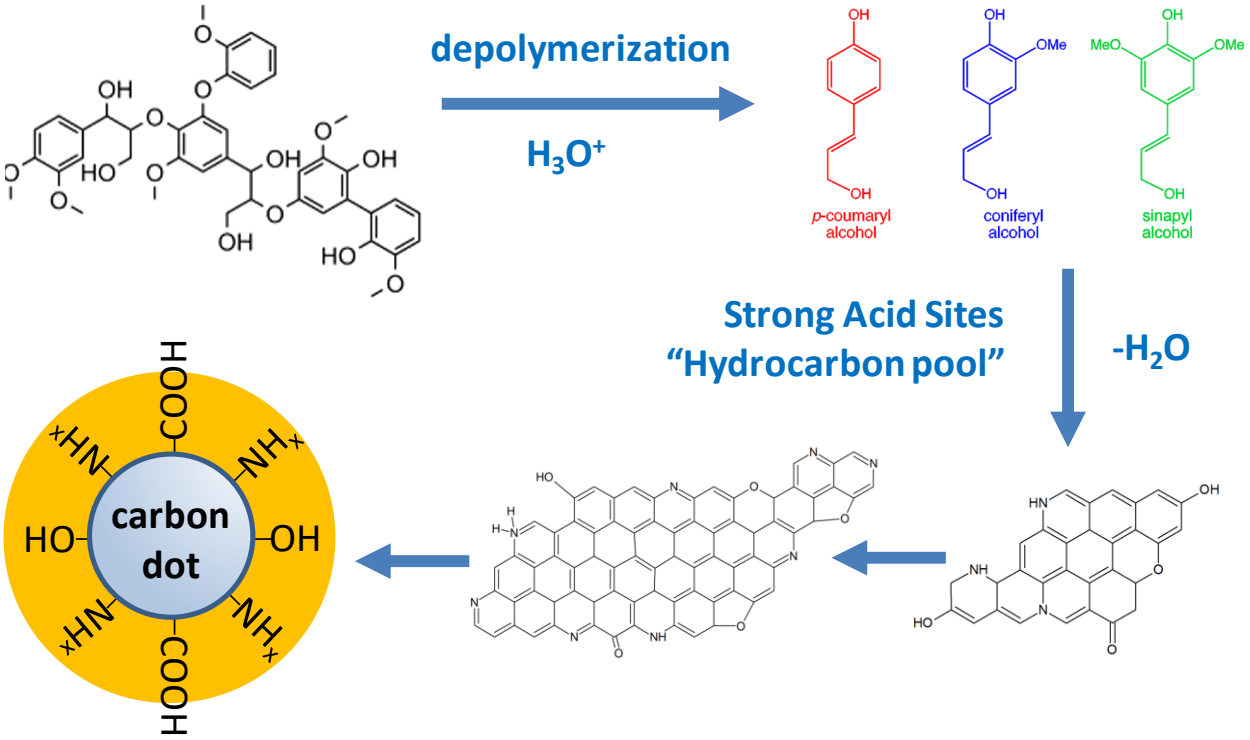

Figure 2. AFM (a), TEM (b), and HR TEM (c) images of lignin carbon dots. The line in panel (a) indicates the location for the C-QD height profile attached below the AFM image. The inset of panel (c) is the electron diffraction pattern of C-QDs in the HR TEM image.

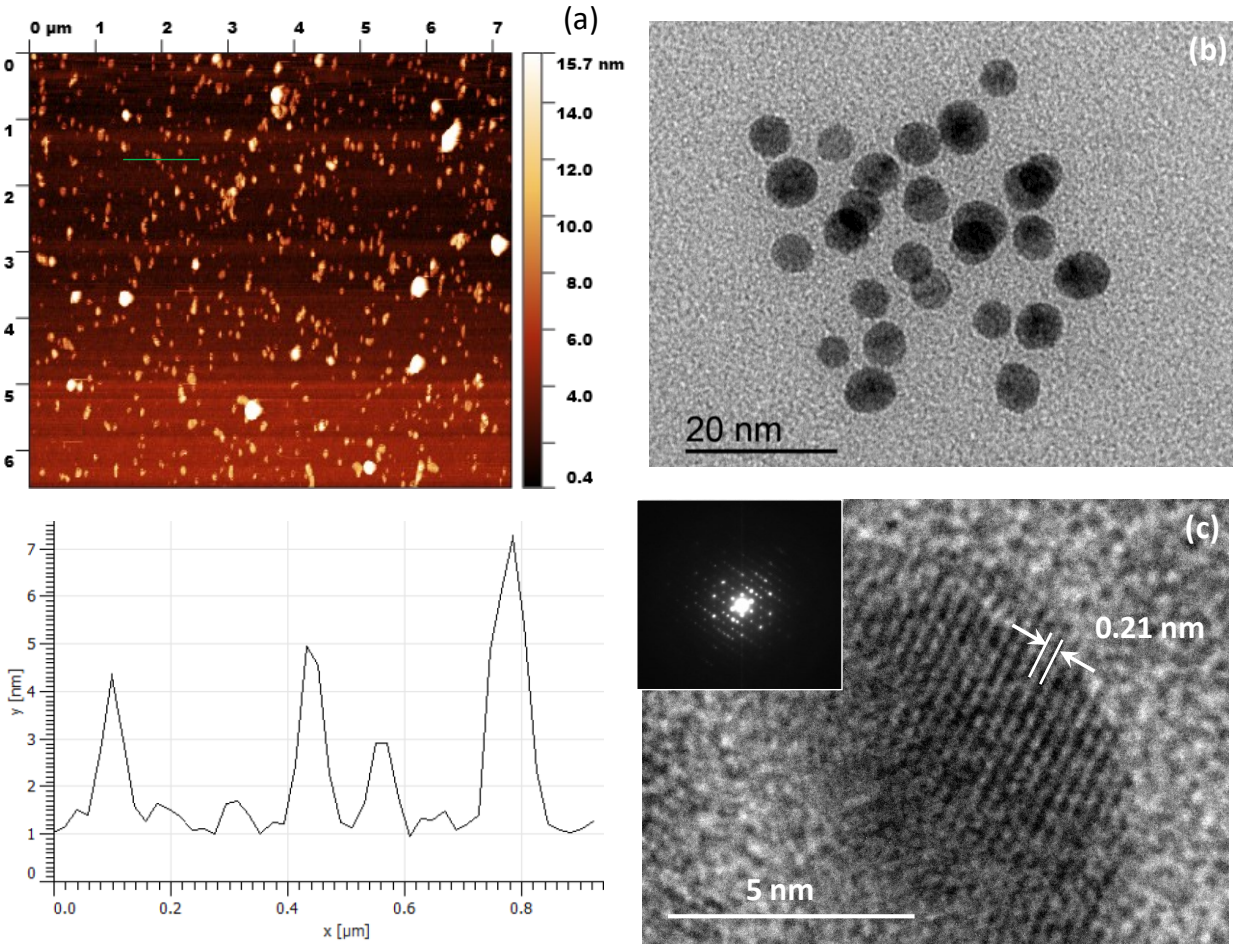

Figure 3. XPS spectra of lignin carbon dots: (a) survey scan, (b-d) detailed scans of O 1s (b), C 1s (c), and (d) N 1s. The spectra of lignin are also added for comparison purpose.

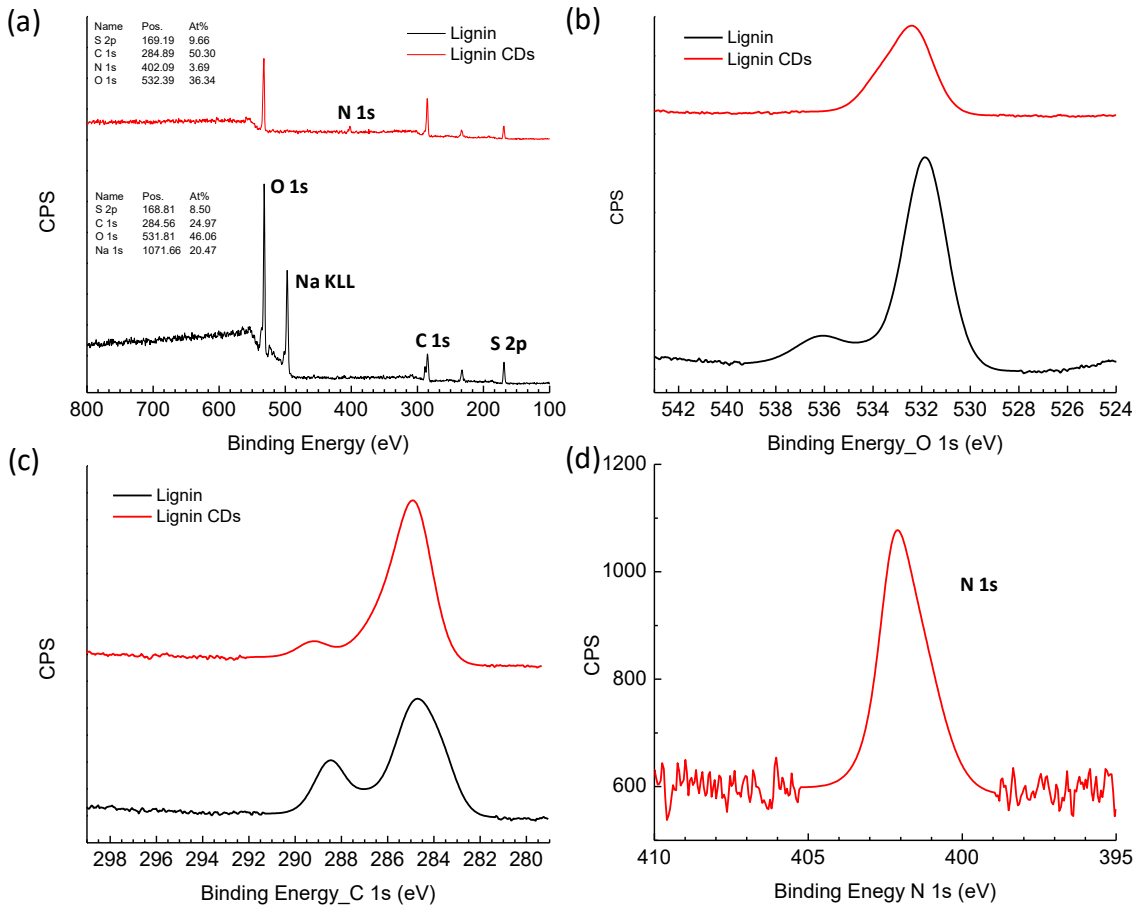

Figure 4. (a) FTIR and (b) Raman spectra of lignin carbon dots. The spectra of lignin are also added for comparison purpose.

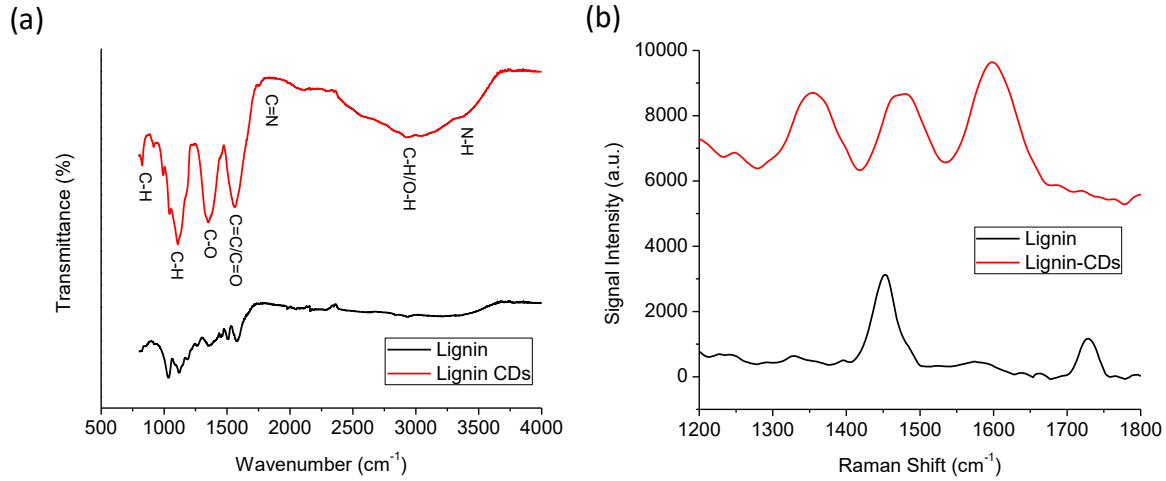

Figure 5. The steady-state emission spectra of lignin carbon dots collected at different dilution samples with an excitation laser of 360 nm (a) and for a 25% diluted sample under different excitation wavelengths (b). The photoluminescence signal (c) and dependence (d) of the as-prepared lignin carbon dot samples with various pH values with 360 nm laser excitation.

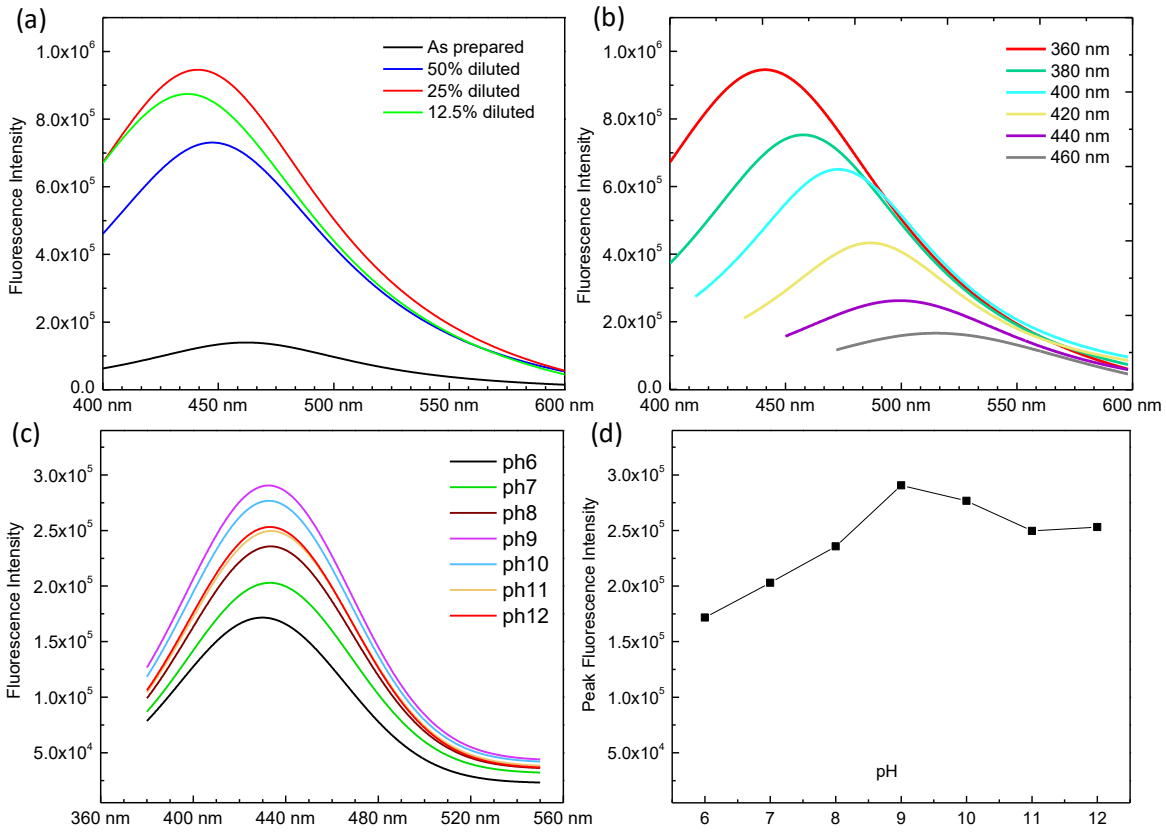

Figure 6. Acidity and temperature effects of hydrothermal synthesis of lignin carbon dots on their photoluminescence signals. (a) Various nitric acid amounts added in the aqueous lignin solution; (b) various hydrothermal synthesis temperature conditions.

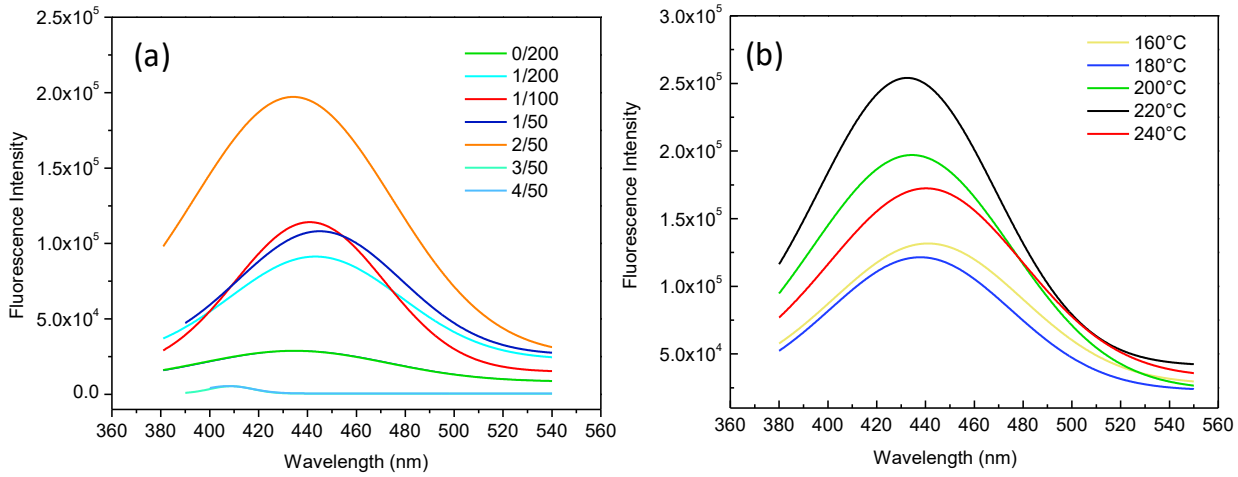

Figure 7. The cell uptake after one-hour incubation (a) and cell viability (b) of N27 cells after one-day incubation with lignin carbon dots samples from a serial dilution of the as-prepared solution. (c) Confocal microscope images of subcellular distribution of lignin carbon dots after N27 cell internalization.

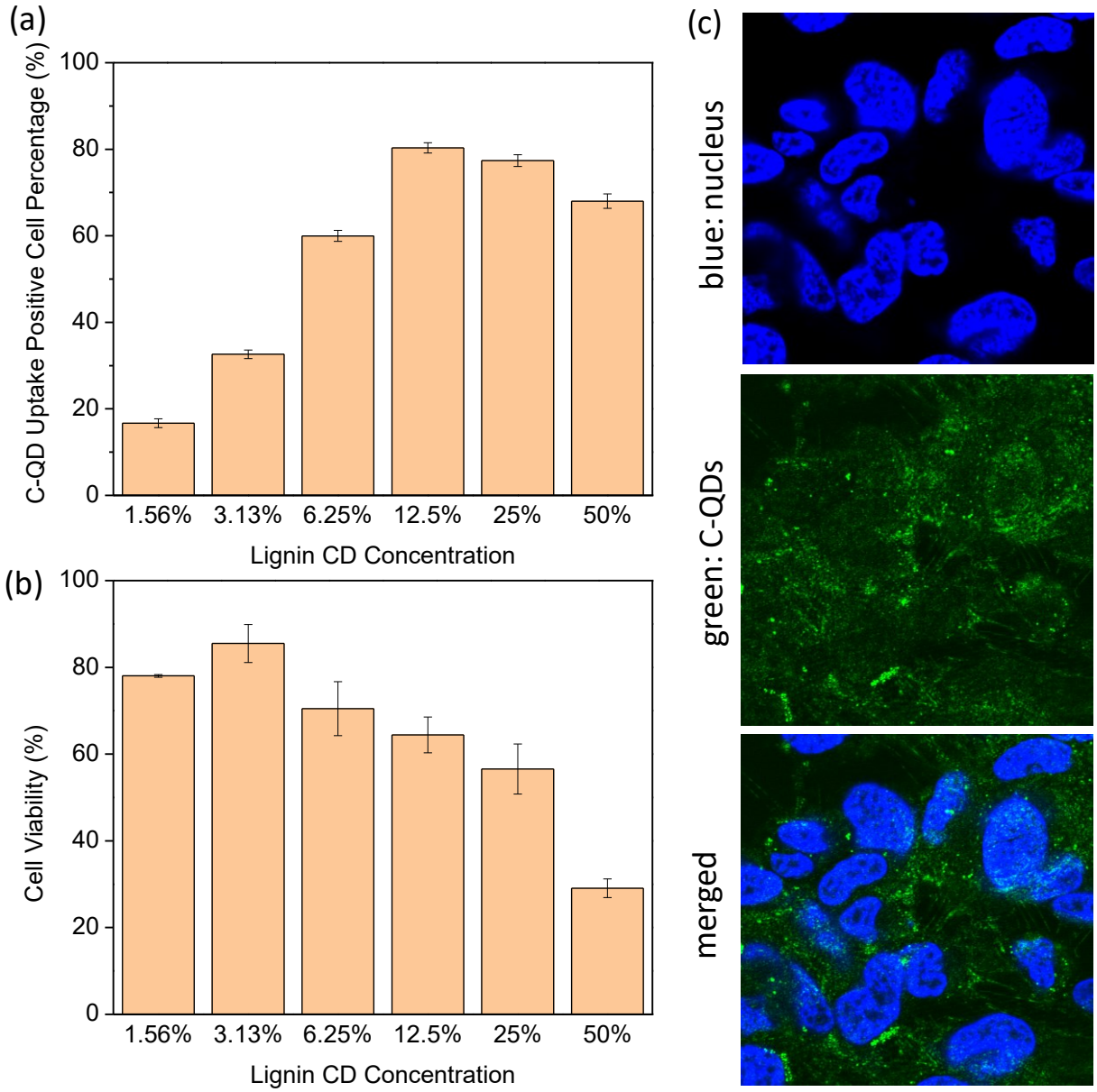

Supplemental Materials

Production of Carbon Dots from Kraft Lignin with Inorganic Acid Catalyst

Yixian Pei[‡a], *An-Yi Chang*[‡a], *Xuan Liu*[a], *Hua Wang*[b], *Hongbo Zhang*[c], *Adarsh Radadia*[a], *Yuxin Wang**[a], *William Yu **[b] *and Shengnian Wang **[a]

[a]*Chemical Engineering, Institute for Micromanufacturing, Center for Biomedical Engineering and Rehabilitations, Louisiana Tech University, PO Box 10137, Ruston, Louisiana, 71272 USA.*

[b]*Chemistry and Physics, Louisiana State University, Shreveport, Louisiana, 71115, USA.*

[c]*Department of Microbiology and Immunology, LSU Health Sciences Center, Shreveport, Louisiana, 71104, USA*

‡ These authors contribute equally to this work.

* Corresponding authors.

Shengnian Wang: Tel: 1-318-257-5125; Email: swang@latech.edu

William Yu, Tel: 1-318-797-5087; Email: wyu6000@gmail.com

Yuxin Wang, Tel: 1-318-278-0108; Email: w-yuxin@hotmail.com

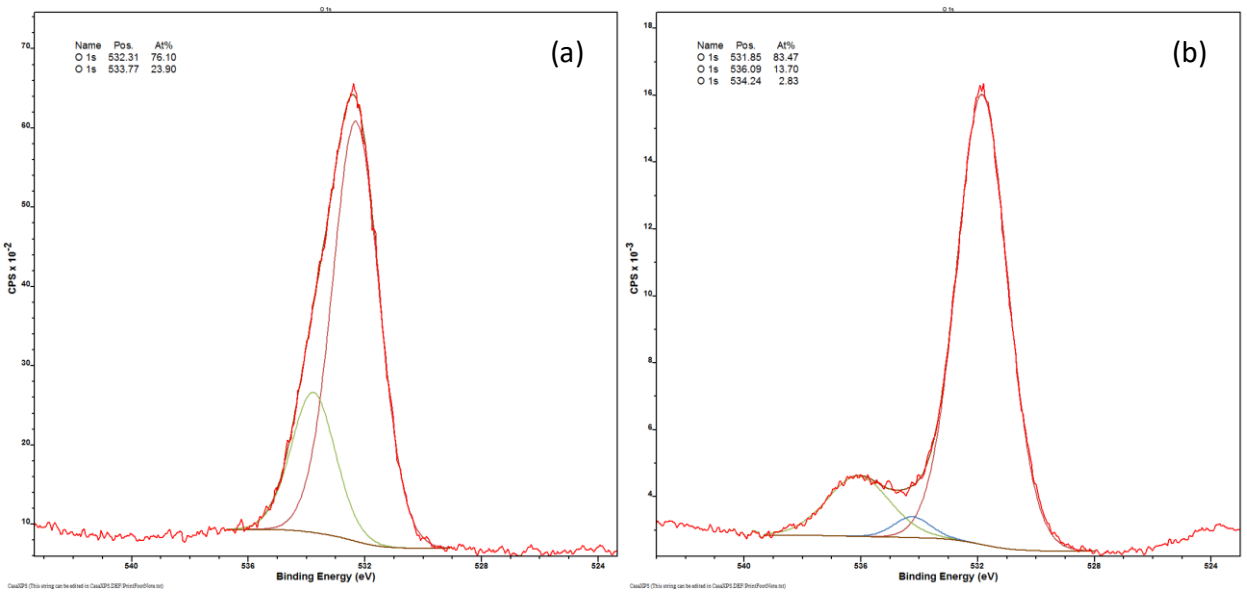

Supp Figure S1. Deconvoluted peaks in the high-resolution O 1s XPS spectra: (a) lignin C-QDs and Kraft lignin (b).

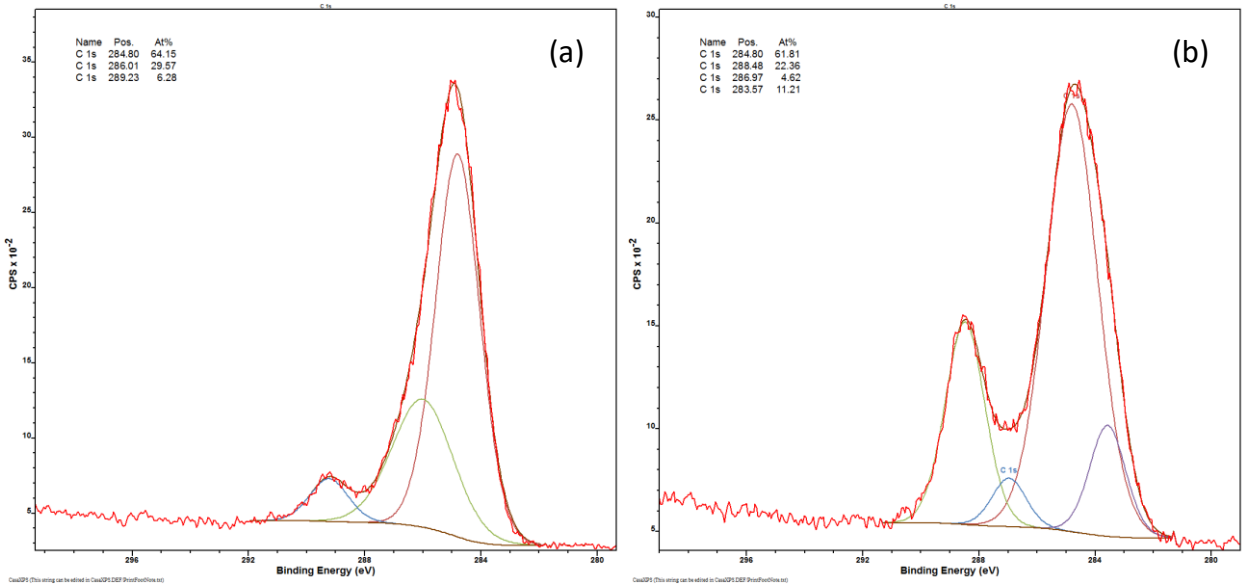

Supp Figure S2. Deconvoluted peaks in the high-resolution C 1s XPS spectra: (a) lignin C-QDs and Kraft lignin (b).

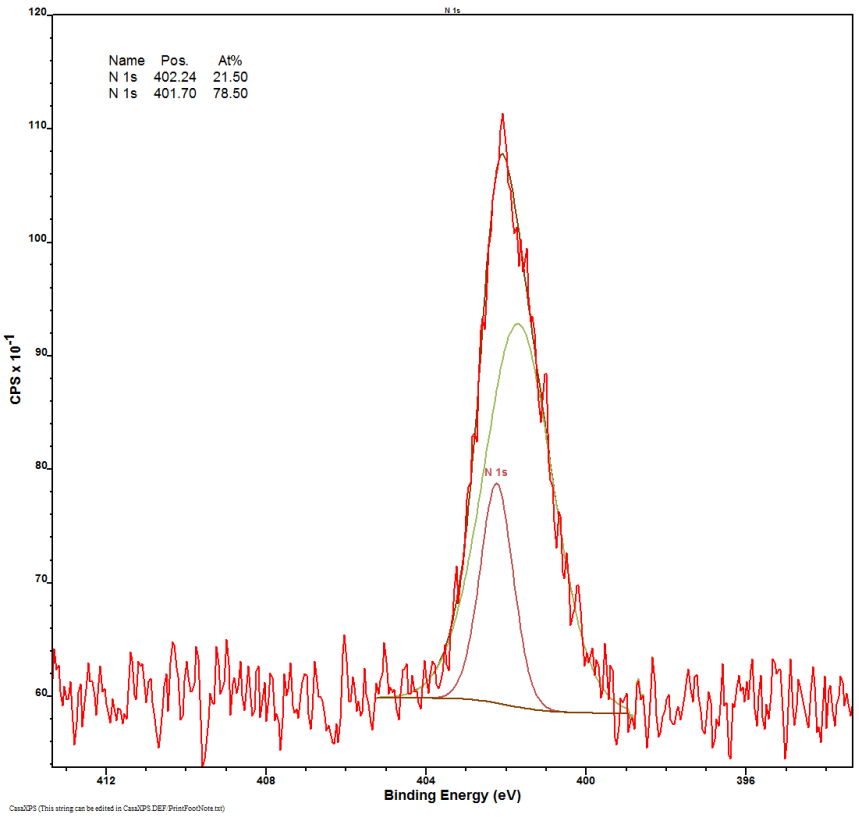

Supp Figure S3. Deconvoluted N 1s peaks in the high-resolution XPS spectrum of lignin C-QDs.

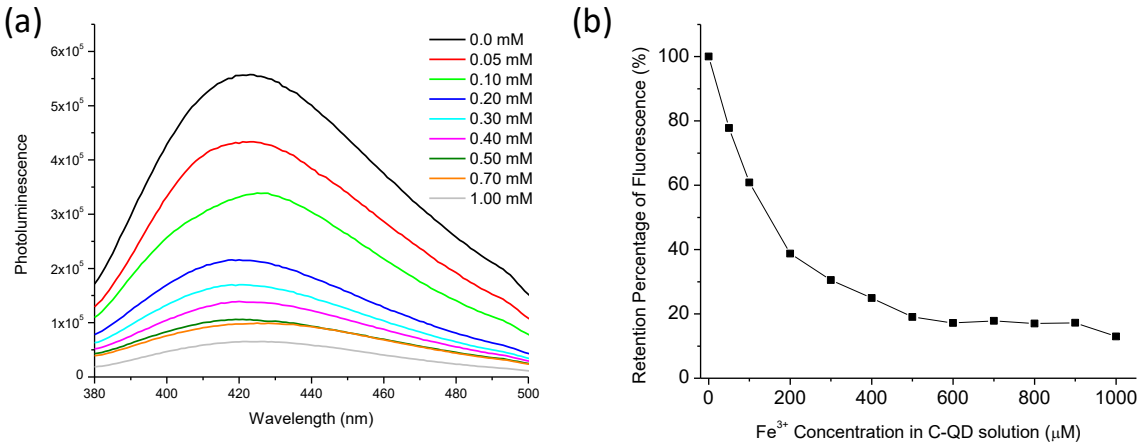

Supp Figure S4. Photoluminescence quenching of lignin C-QDs (30 ng mL-1) at the interference of Fe^{3+} ions in C-QD solutions: (a) Photoluminescence spectra; (b) the fluorescence signal retention percentage of C-QD samples with a concentrations of Fe^{3+} ions at 0, 0.05, 0.10, 0.20, 0.30, 0.40, 0.50, 0.70, and 1.00 mM.